

Supporting Information for “A weakly structured stem for human origins in Africa”

Aaron P. Ragsdale, Timothy D. Weaver, Brenna M. Henn, and Simon Gravel

January 2, 2022

Contents

1	Data and sequencing	2
1.1	Sequencing and variant calling	2
1.2	Nama sample collection and consent	2
1.3	Details about populations used in analyses	2
1.4	Filtering and subsetting data	3
2	Computing statistics	3
2.1	LD and diversity statistics used in model fits	3
2.2	Computing LD and diversity statistics	3
2.3	Estimating two-locus statistics with small sample sizes	4
2.4	Computing conditional SFS	4
3	Model specification and fitting	4
3.1	General strategy for building models and introducing complexity	5
3.2	Optimization using moments	5
3.3	Confidence intervals using Godambe methods	5
4	Gene genealogy reconstruction	6
5	Predictions from inferred demographic models	6
5.1	F_{ST} between coexisting populations over time	6
5.2	f_4 statistics between pairs of contemporary and pairs of ancient populations	6
6	Validations using simulatinos from inferred demographic models	6
6.1	Simulation details	6
6.2	cSFS prediction under inferred models	6
6.3	Relate curves from inferred models	6
6.4	Distribution of deep branch affinities to Neanderthal sequence	6
6.5	Mutation versus recombination rates	6
	References	7
	Supporting tables	8
	Supporting figures	12

1 Data and sequencing

1.1 Sequencing and variant calling

Low coverage (4-8x) Illumina short read data were generated for the Nama, Gumuz, Amhara and Oromo populations as part of the African Diversity Reference Panel (Sanger / Wellcome Trust) (GURDASANI *et al.*, 2015; PAGANI *et al.*, 2015) and approved through a secondary data analysis agreement for this project. Briefly, raw reads were aligned to GRCH37 with BWA-mem [APR: cite](#), duplicates marked with Picard MarkDuplicates, reads were realigned around indels with GATK RealignerTargetCreator / IndelRealigner followed by BQSR with dbSNP 137. Contamination checks were performed requiring that FREEMIX < 0.05; contamination checks resulted in the elimination of 22 Nama samples. We note that the high heterozygosity in these genomes both due to inherent genetic diversity and admixture may have violated base assumptions for this heterozygosity check. Genomes were then variant called with GATK3.2 Unified Genotyper [APR: cite](#) using joint calling across 2,478 individuals within the ADRP dataset with a minimum base quality of 17. Data were merged with 1000 Genomes Phase 3 (1000 GENOMES PROJECT CONSORTIUM *et al.*, 2015) using the union of sites identified with bcftools isec (-n+1) [APR: cite](#) then refined with Variant Recalibrator with a truth sensitivity threshold of 99.5%. HapMap III and dbSNP 138 served as known sites while 1000 Genomes Phase 1 Omni2.5 and Phase 1 genomic SNP served as the training set. After VR, no batch effects were observed along PC1 and PC2 for 1000 Genomes vs. ADRP. Phasing on the combined dataset was performed via SHAPEIT2 [APR: cite](#) and utilized the duoHMM option for duos and trios. We highlight 82 Nama genomes which are newly available (unpublished) under accession number EGAD00001006198. Among these 82 Nama samples, we down-sampled the individuals to minimize close relatives and admixture, such that 44 Nama genomes were retained. 2nd and 3rd degrees relatives were inferred from reconstructed pedigrees with Omni2.5 SNP array data. Individuals with > 70% estimated Khoe-San ancestry were retained for analysis, after partitioning ancestry into $k = 6$ clusters with ADMIXTURE [APR: cite](#) where alternative ancestries represent European, West African, Near Eastern, and East African gene flow.

1.2 Nama sample collection and consent

DNA samples were collected from three Nama communities in the Richtersveld region of South Africa, which borders southern Namibia, in 2012. A community guide was present during each interview and facilitated consent in Afrikaans or Nama. Written consent was recorded per our IRB protocol with human subjects approval from Stanford University (Protocol #13829), Stellenbosch University (N11/07/210) and later maintained via SUNY Stony Brook (Protocol #727494). Saliva samples were extracted from Oragene [OGR-500] kits at Stellenbosch University. Results stemming from genetic analyses have been communicated in 2015, 2019, 2021 via community presentations, a radio interview and to representatives of the Richtersveld National Park.

1.3 Details about populations used in analyses

SG: To be expanded. TODO: Brenna

- From the merged dataset of the African Diversity Reference Panel and 1000 Genomes phase 3 data, subsampled to population included in this study
- West Africa: Mende from Sierra Leone (MSL); South Africa: newly sequenced Nama; East Africa: Gumuz (traditionally hunter-gatherer with low levels of Eurasian admixture), Oromo and Amhara (combined as traditionally agriculturalists with large proportion of back-to-Africa Eurasian ancestry); Eurasian: British (GBR)
- Combined with the high coverage Vindija neanderthal genome

- For running Relate, we used a larger set of populations. We kept all African 1000 Genomes populations, along with the Nama, Gumuz, Oromo, and Amhara, as well as 4 Eurasian populations from 1000 Genomes: GBR, CEU, PJL, and CHB

1.4 Filtering and subsetting data

All analyses presented in this work focus on biallelic single nucleotide polymorphisms within the 1000 Genomes Phase 3 strict mask.

For the moments-LD analysis, we focused on intergenic locations because these appear less affected by natural selection compared to both synonymous and nonsynonymous variation (RAGSDALE *et al.*, 2018). To enable comparison with Neanderthal DNA, we excluded regions for which the Vindija Neanderthal sample had less than 100 contiguous base pairs.

2 Computing statistics

2.1 LD and diversity statistics used in model fits

APR: D^2 , D_z , π_2 , and H . Definitions, notation, indexing...

2.2 Computing LD and diversity statistics

We compared single- and two-locus statistics in the data to predictions based on detailed demographic models. Model predictions were obtained using recursions described in RAGSDALE and GRAVEL (2019) and implemented in the software *moments.LD* (<https://bitbucket.org/simongravel/moments/src/main/>). The model computes expected patterns of single-nucleotide pairwise diversity and linkage disequilibrium as a function of recombination distance between variants within and across populations, under the assumption of neutrality.

For numerical convenience, observed genetic variants were binned by recombination distances. We assessed the robustness of the statistics to errors in the recombination maps by considering two different recombination maps, the OMNI YRI and HapMapII (1000 GENOMES PROJECT CONSORTIUM *et al.*, 2015; INTERNATIONAL HAPMAP CONSORTIUM *et al.*, 2007). Statistics were largely unchanged by using a different map (Figure ??). APR: These maps are both inferred using array data, which is sparse. Comment on this.

We removed bins of recombination distance less than a recombination distance of $r = 5 \times 10^{-6}$ (at a rough estimate of 1 cM/Mb, this corresponds to a minimum distance of 500 bp on average) to avoid previously reported biases at short distances due to processes like multinucleotide mutations (HARRIS and NIELSEN, 2014; RAGSDALE and GRAVEL, 2019). To avoid uncertainty in phasing, we used unphased genotypes to compute LD statistics, as proposed in RAGSDALE and GRAVEL (2020).

Finally, we estimated uncertainty due to the finite amount of genetic material used in inference using bootstrap over 500 segments along the genome with roughly equal lengths of retained sequences within each segment. First, for each distance bin, we used these bootstrap samples to obtain a variance-covariances matrix across all statistics. This variance-covariance matrix was used to obtain a model likelihood for each recombination distance bin and single-locus nucleotide diversity, as a multivariate Gaussian likelihood. The full model likelihood was taken as the product of likelihoods over each bin. In other words, we optimized a composite likelihood where observations in different bins were taken to be independent. To account for correlations across bins in uncertainty estimates, we estimated parameter confidence intervals using the same bootstrap set using the Godambe information matrix (COFFMAN *et al.*, 2016). SG: is redundancy here with section "Optimization using moments". I think we can get rid of this and say: "optimization and uncertainty calculations are described in section "Optimization using moments"?", This may be a bit more complicated, since the Optimizatino section relies on this description. I think we should just punt the bootstrap description to that section. TODO: discuss Aaron + Simon

2.3 Estimating two-locus statistics with small sample sizes

The approach from RAGSDALE and GRAVEL (2020) provides unbiased estimates of the LD statistics considered here, with smaller sample sizes causing greater uncertainty in the estimated statistics, but is accounted for by computing variances/covariances via bootstrap. **SG: I don't think that this is true if our bootstrap is over genomic regions. In an infinite genome with a tiny sample size, we would estimate no uncertainty... Or at least, it is only true if the Neanderthal form a truly randomly mating population...**

Some statistics, such as D^2 , require at least two diploid samples to compute. Since we used a single Neanderthal sample, these statistics for the Neanderthal population were not used in the fit. By contrast, there are statistics that only require a single sample per population to estimate. These include cross-population heterozygosity, as well as some statistics involving more than one population. For example, statistics of the form $D_{human}(1 - 2p_{human})(1 - 2q_{neanderthal})$ require a single Neanderthal sample and are informative of the Neanderthal demography. These statistics were included in the fit, but statistics requiring more than one Neanderthal sample to estimate were removed.

2.4 Computing conditional SFS

The conditional site frequency spectrum (or cSFS) is the distribution of allele frequencies restricted to loci that satisfy a given condition. Specifically, we consider the distribution of allele frequencies in present-day populations conditioned on the Vindija Neanderthal carrying the derived allele relative to the inferred ancestral allele. Ancestral alleles were determined from a 6 primate alignment **APR: cite**. This cSFS is expected to be close to uniform under neutrality and a simple split model (with no subsequent migration) between the ancestors of modern humans and Neanderthal (CHEN *et al.*, 2007). By contrast, a U-shaped distribution has been taken as evidence for archaic introgression from a population whose split from modern humans is at least as old as that of the human-Neanderthal split DURVASULA and SANKARARAMAN (2020); YANG *et al.* (2012). Because we wanted to compare our inferences (based on intergenic sites) to inferences from previous work (based on whole-genome data), we computed the cSFS for both intergenic and all sites genome-wide. Sites with no calls in the Vindija Neanderthal were excluded from this analysis. **APR: Figures XX.**

Because we were concerned that cSFS analyses may be affected by incorrect inference of the ancestral allele HERNANDEZ *et al.* (2007), we computed the cSFS for all mutations, and for transitions and transversions separately **APR: (Figure X, cSFS)**. Comparisons of these observed cSFS with model predictions are discussed in the model prediction section below.

3 Model specification and fitting

For the early history, we tested model parameterizations that cover many of the proposed scenarios of population structure, size changes, and/or archaic admixture. The simplest model, in terms of number of parameters, was a single-origin expansion of modern humans, with no structure in the stem and no archaic admixture aside from the Neanderthal admixture in Eurasian populations following the out-of-Africa migration. This model allowed for a population size change in the stem of modern humans between the ancestral split of the human-Neanderthal lineages and the more recent split of branches leading to Southern and West/Eastern African populations.

To include population structure in early human history, we considered multiple parameterizations of models that allowed more than a single stem population. In general, stem populations were allowed to vary in their sizes, split times, and migration rates, with parameterizations flexible enough to encompass proposed scenarios of either archaic admixture or population structure, both connected by gene flow or with isolation between stems.

In one parameterization of early structure, which we refer to as a “continuous migration” model, a secondary stem population (stem 2) split from the primary stem (stem 1) that leads to modern humans. Stem 1 contributed to present-day populations via a series of population splits similar to the single-origin model,

while stem 2 contributed through continuous symmetric migrations with contemporaneous populations. The symmetrical migration rates could differ across population pairs and over different epochs. This continuous migration was allowed until stem 2 disappeared, which occurred as recently as 5kya. We tested models that both allowed or disallowed migration between stems, i.e., before stem 1 split into S/E/W African populations.

In another parameterization of early structure, a secondary stem population (stem 2) contributed ancestry to present-day populations via a series of instantaneous admixture events (i.e., pulse admixture or “merger” events) to lineages leading to sampled present-day African populations. Merger events were allowed to occur in one or more of the Nama, Mende, and Gumuz branches, as well as the branch of East and West Africans prior to their split. Those admixture events were allowed to occur at any time along those branches, and with any proportions, and stem 2 was allowed to split from the primary stem at any time before subsequent divergences (and either before or after the split of the Neanderthal branch). We tested models that allowed migration between the early stems, before subsequent splits and admixture events, as well as models that were restricted to isolation between stem branches. Depending on the specific parameters, such models encompass commonly-considered ghost archaic admixture scenarios (e.g., if a long-isolated lineage more recently contributes a minority of ancestry to one or more populations), as well as relatively simple fragmentation-coalescence scenarios.

Based on the geographical locations of present-day populations, we tentatively labeled ancestral branches using a parsimony in migration, referring to South, East, and West African branches (S/E/W AFR, Figure X). We do not know the geographical location of these ancestral populations (nor even if they correspond to populations with a well-defined geographic range), and these labels should be considered as tentative. However, we found it useful to name branches in reference to where in Africa their descendants are found.

SG: Please double-check this paragraph! TODO Brenna?

3.1 General strategy for building models and introducing complexity

3.2 Optimization using moments

moments-LD uses a composite likelihood approach to simultaneously fit relative pairwise diversity and LD statistics over a range of recombination distances. Likelihoods were computed independently for pairwise diversity and each recombination distance bin using a multivariate Gaussian likelihood function as described in Section 2.2. These were multiplied across bins and the single set of heterozygosity statistics following the approach detailed in RAGSDALE and GRAVEL (2019). For each model tested, we ran multiple rounds of optimization, alternating between the *optimize_log_fim*, *optimize_log_powell*, and *optimize_lbfgsb* methods to explore parameter space and hone in on the best fit parameters. Initial guesses for parameters were chosen from demographically plausible starting points and then perturbed to explore space, using gradient descent (on the log of the parameters). The best fits from these initial rounds of optimization were then chosen as the starting points for optimization using the Powell and/or the L-BFGS-B methods (as implemented in the SciPy optimization package VIRTANEN *et al.* (2020)). This process was repeated with alternating optimization methods until the best fit parameter set converged consistently.

3.3 Confidence intervals using Godambe methods

The bootstrap replicates that were used to compute the variance-covariance structure of the observed statistics within bins were also used to build 500 bootstrap replicates of the data by resampling with replacement. For the best fit parameters, we computed confidence intervals using the Godambe Information approach, which corrects composite likelihood estimates of confidence intervals to account for nonindependence in the data, including linkages between loci and nonindependence of recombination bins COFFMAN *et al.* (2016).

- 4 Gene genealogy reconstruction
- 5 Predictions from inferred demographic models
 - 5.1 F_{ST} between coexisting populations over time
 - 5.2 f_4 statistics between pairs of contemporary and pairs of ancient populations
- 6 Validations using simulatinos from inferred demographic models
 - 6.1 Simulation details
 - 6.2 cSFS prediction under inferred models
 - 6.3 Relate curves from inferred models
 - 6.4 Distribution of deep branch affinities to Neanderthal sequence
 - 6.5 Mutation versus recombination rates

References

- 1000 GENOMES PROJECT CONSORTIUM, A. AUTON, L. D. BROOKS, R. M. DURBIN, E. P. GARRISON, *et al.*, 2015 A global reference for human genetic variation. *Nature* **526**: 68–74.
- CHEN, H., R. E. GREEN, S. PÄÄBO, and M. SLATKIN, 2007 The joint allele-frequency spectrum in closely related species. *Genetics* **177**: 387–398.
- COFFMAN, A. J., P. H. HSIEH, S. GRAVEL, and R. N. GUTENKUNST, 2016 Computationally efficient composite likelihood statistics for demographic inference. *Mol. Biol. Evol.* **33**: 591–593.
- DURVASULA, A., and S. SANKARARAMAN, 2020 Recovering signals of ghost archaic introgression in african populations. *Sci Adv* **6**: eaax5097.
- GURDASANI, D., T. CARSTENSEN, F. TEKOLA-AYELE, L. PAGANI, I. TACHMAZIDOU, *et al.*, 2015 The african genome variation project shapes medical genetics in africa. *Nature* **517**: 327–332.
- HARRIS, K., and R. NIELSEN, 2014 Error-prone polymerase activity causes multinucleotide mutations in humans. *Genome Res.* **24**: 1445–1454.
- HERNANDEZ, R. D., S. H. WILLIAMSON, and C. D. BUSTAMANTE, 2007 Context dependence, ancestral misidentification, and spurious signatures of natural selection. *Mol. Biol. Evol.* **24**: 1792–1800.
- INTERNATIONAL HAPMAP CONSORTIUM, K. A. FRAZER, D. G. BALLINGER, D. R. COX, D. A. HINDS, *et al.*, 2007 A second generation human haplotype map of over 3.1 million SNPs. *Nature* **449**: 851–861.
- PAGANI, L., S. SCHIFFELS, D. GURDASANI, P. DANECEK, A. SCALLY, *et al.*, 2015 Tracing the route of modern humans out of africa by using 225 human genome sequences from ethiopians and egyptians. *Am. J. Hum. Genet.* **96**: 986–991.
- RAGSDALE, A. P., and S. GRAVEL, 2019 Models of archaic admixture and recent history from two-locus statistics. *PLoS Genet.* **15**: e1008204.
- RAGSDALE, A. P., and S. GRAVEL, 2020 Unbiased estimation of linkage disequilibrium from unphased data. *Mol. Biol. Evol.* **37**: 923–932.
- RAGSDALE, A. P., C. MOREAU, and S. GRAVEL, 2018 Genomic inference using diffusion models and the allele frequency spectrum. *Curr. Opin. Genet. Dev.* **53**: 140–147.
- VIRTANEN, P., R. GOMMERS, T. E. OLIPHANT, M. HABERLAND, T. REDDY, *et al.*, 2020 SciPy 1.0: fundamental algorithms for scientific computing in python. *Nat. Methods* **17**: 261–272.
- YANG, M. A., A.-S. MALASPINAS, E. Y. DURAND, and M. SLATKIN, 2012 Ancient structure in africa unlikely to explain neanderthal and non-african genetic similarity. *Mol. Biol. Evol.* **29**: 2987–2995.

Supporting tables

Table S1: **Best-fit parameters from the Single-Origin model.** APR: fill in caption - generation time of 29 years, other details

Parameter	Description	Value	Std. err.
N_e	Ancestral effective population size	10198	403
N_{MH}	Size of modern-human lineage between Neanderthal and Nama splits	21111	529
N_{Nama_0}	Initial Nama size	10224	370
N_{Nama_F}	Final Nama size	222	9
N_{MSL_0}	Initial Mende size	17211	769
N_{MSL_F}	Final Mende size	16822	606
N_{EA}	Size of East African branch	7139	273
N_{Gumuz_F}	Final Gumuz size	3831	131
N_{EP}	East African agriculturist size	13033	491
N_{GBR_0}	Initial British size	846	33
N_{GBR_F}	Final British size	12121	507
N_{Neand}	Neanderthal size	1867	105
T_{Nama}	Nama split time (years)	110400	2525
$m_{Nama-MSL}$	Nama–Mende symmetric migration rate	2.82×10^{-5}	0.158×10^{-5}
$m_{Nama-EA}$	Nama–East Africa symmetric migration rate	4.94×10^{-5}	0.197×10^{-5}
m_{MSL-EA}	Mende–East Africa migration rate	18.76×10^{-5}	0.764×10^{-5}
m_{EA-GBR}	East Africa–Europe migration rate	4.42×10^{-5}	0.239×10^{-5}
m_{EA-EA}	Intra-East Africa migration rate	41.28×10^{-5}	1.33×10^{-5}
$f_{GBR \rightarrow EP}$	Ancestry proportion of East African agriculturalists from GBR 12 ka ($1 - f$ from Gumuz)	0.658	0.0039
$f_{EP \rightarrow Nama}$	Ancestry proportion from EA pastoralists to Nama 2 ka	0.279	0.0039
$f_{GBR \rightarrow Nama}$	Ancestry proportion from Europeans to Nama 10 generations ago	0.150	0.0019

Table S2: **Best-fit parameters from the Continuous-Migration model.** APR: fill in caption - generation time of 29 years, other details

Parameter	Description	Value	Std. err.
N_e	Ancestral effective population size	7270	1777
N_{stem1}	Size of stem 1 lineage between Neanderthal and Nama splits	8256	1612
N_{stem2}	Size of stem 2 lineage	13547	2488
N_{Nama_0}	Initial Nama size	11939	2989
N_{Nama_F}	Final Nama size	221	54
N_{MSL_0}	Initial Mende size	9738	2479
N_{MSL_F}	Final Mende size	28150	6628
N_{EA}	Size of East African branch	7489	1841
N_{Gumuz_F}	Final Gumuz size	3728	915
N_{EP}	East African agriculturist size	13072	3246
N_{GBR_0}	Initial British size	959	231
N_{GBR_F}	Final British size	11822	2889
N_{Neand}	Neanderthal size	2670	591
T_{stems}	Stem split time (years)	1163072	390803
T_{Nama}	Nama split time (years)	134745	17775
$m_{Nama-MSL}$	Nama–Mende symmetric migration rate	0.98×10^{-5}	0.366×10^{-5}
$m_{Nama-EA}$	Nama–East Africa symmetric migration rate	4.08×10^{-5}	1.02×10^{-5}
m_{MSL-EA}	Mende–East Africa migration rate	21.4×10^{-5}	5.32×10^{-5}
m_{EA-GBR}	East Africa–Europe migration rate	4.17×10^{-5}	1.02×10^{-5}
m_{EA-EA}	Intra-East Africa migration rate	33.6×10^{-5}	8.35×10^{-5}
$f_{GBR \rightarrow EP}$	Ancestry proportion of East African agriculturalists from GBR 12 ka ($1 - f$ from Gumuz)	0.642	0.0037
$f_{EP \rightarrow Nama}$	Ancestry proportion from EA pastoralists to Nama 2 ka	0.255	0.0043
$f_{GBR \rightarrow Nama}$	Ancestry proportion from Europeans to Nama 10 generations ago	0.156	0.0021
m_{stems}	Stem 1–stem 2 migration rate	6.43×10^{-5}	1.05×10^{-5}
$m_{stem2-Nama}$	Stem 2–Nama migration rate	5.82×10^{-5}	1.60×10^{-5}
$m_{stem2-MSL}$	Stem 2–Mende migration rate	16.4×10^{-5}	4.19×10^{-5}
$m_{stem2-EA}$	Stem 2–East Africa migration rate	3.10×10^{-5}	0.901×10^{-5}

Table S3: **Best-fit parameters from the Merger-Without-Stem-Migration model.** APR: fill in caption - generation time of 29 years, other details

Parameter	Description	Value	Std. err.
N_e	Ancestral effective population size	11258	326
N_{stem1}	Size of stem 1 lineage between stem 1–stem 2 split and stem 1E–stem 1S split	113	76
N_{stem2}	Size of stem 2 lineage	23984	1149
N_{Nama0}	Initial Nama and stem 1S size	13134	384
N_{NamaF}	Final Nama size	225	7.3
N_{MSL0}	Initial Mende size	11856	322
N_{MSLF}	Final Mende size	25558	987
N_{EA}	Size of East African and stem 1E branch	9136	246
N_{GumuzF}	Final Gumuz size	3385	102
N_{EP}	East African agriculturist size	13650	408
N_{GBR0}	Initial British size	931	29
N_{GBRF}	Final British size	12064	334
N_{Neand}	Neanderthal size	1935	91
T_{stems}	Stem split time (years)	420881	27380
T_{stem1}	Stem 1 split time into stem 1E and stem 1S (years)	367434	19952
$m_{Nama-MSL}$	Nama–Mende symmetric migration rate	0.361×10^{-5}	0.113×10^{-5}
$m_{Nama-EA}$	Nama–East Africa symmetric migration rate	4.00×10^{-5}	0.130×10^{-5}
m_{MSL-EA}	Mende–East Africa migration rate	19.5×10^{-5}	0.548×10^{-5}
m_{EA-GBR}	East Africa–Europe migration rate	3.77×10^{-5}	0.152×10^{-5}
m_{EA-EA}	Intra-East Africa migration rate	37.1×10^{-5}	1.26×10^{-5}
$f_{GBR \rightarrow EP}$	Ancestry proportion of East African agriculturalists from GBR 12 ka ($1 - f$ from Gumuz)	0.647	0.0037
$f_{EP \rightarrow Nama}$	Ancestry proportion from EA pastoralists to Nama 2 ka	0.257	0.0042
$f_{GBR \rightarrow Nama}$	Ancestry proportion from Europeans to Nama 10 generations ago	0.156	0.0021
T_{Nama}	Time of Nama merger event	117392	8253
$f_{stem2 \rightarrow Nama}$	Proportion of stem 2 ancestry making up initial Nama lineage ($1 - f$ from stem 1S)	0.707	0.0086
T_{EA}	Time of East Africa merger event	94892	3648
$f_{stem2 \rightarrow EA}$	Proportion of stem 2 ancestry making up initial East Africa lineage ($1 - f$ from stem 1E)	0.481	0.0074
T_{MSL}	Time of secondary admixture from stem 2 to Mende	23922	570
$f_{stem2 \rightarrow MSL}$	Proportion of ancestry from secondary stem 2 admixture to Mende	0.168	0.0036

Table S4: **Best-fit parameters from the Merger-With-Stem-Migration model.** APR: fill in caption
- generation time of 29 years, other details

Parameter	Description	Value	Std. err.
N_e	Ancestral effective population size	11479	1369
N_{stem1}	Size of stem 1 lineage between Neanderthal split and stem 1E–stem 1S split	117	838
N_{stem2}	Size of stem 2 lineage	24393	6668
N_{Nama0}	Initial Nama size	13211	1514
N_{NamaF}	Final Nama size	223	31
N_{MSL0}	Initial Mende size	11444	1165
N_{MSLF}	Final Mende size	27417	4332
N_{EA}	Size of East African Branch	9077	1628
N_{GumuzF}	Final Gumuz size	3402	337
N_{EP}	East African agriculturist size	13506	1684
N_{GBR0}	Initial British size	953	122
N_{GBRF}	Final British size	12406	1678
N_{Neand}	Neanderthal size	2416	235
T_{stems}	Stem split time (years)	1442022	426449
T_{stem1}	Stem 1S–stem 1E split time (years)	479401	166339
$m_{Nama-MSL}$	Nama–Mende symmetric migration rate	0.712×10^{-5}	0.401×10^{-5}
$m_{Nama-EA}$	Nama–East Africa symmetric migration rate	4.35×10^{-5}	0.912×10^{-5}
m_{MSL-EA}	Mende–East Africa migration rate	19.8×10^{-5}	2.57×10^{-5}
m_{EA-GBR}	East Africa–Europe migration rate	3.87×10^{-5}	0.550×10^{-5}
m_{EA-EA}	Intra-East Africa migration rate	35.9×10^{-5}	5.36×10^{-5}
$f_{GBR \rightarrow EP}$	Ancestry proportion of East African agriculturalists from GBR 12 ka ($1 - f$ from Gumuz)	0.640	0.0075
$f_{EP \rightarrow Nama}$	Ancestry proportion from EA pastoralists to Nama 2 ka	0.257	0.0049
$f_{GBR \rightarrow Nama}$	Ancestry proportion from Europeans to Nama 10 generations ago	0.157	0.0031
m_{stems}	Stem 1–stem 2 migration rate	11.6×10^{-5}	8.74×10^{-5}
T_{Nama}	Time of Nama merger event	118547	28170
$f_{stem2 \rightarrow Nama}$	Proportion of stem 2 ancestry making up initial Nama lineage ($1 - f$ from stem 1S)	0.714	0.067
T_{EA}	Time of East Africa merger event	98083	8865
$f_{stem2 \rightarrow EA}$	Proportion of stem 2 ancestry making up initial East Africa lineage ($1 - f$ from stem 1E)	0.495	0.059
T_{MSL}	Time of secondary admixture from stem 2 to Mende	25119	641
$f_{stem2 \rightarrow MSL}$	Proportion of ancestry from secondary stem 2 admixture to Mende	0.181	0.0085

Supporting figures

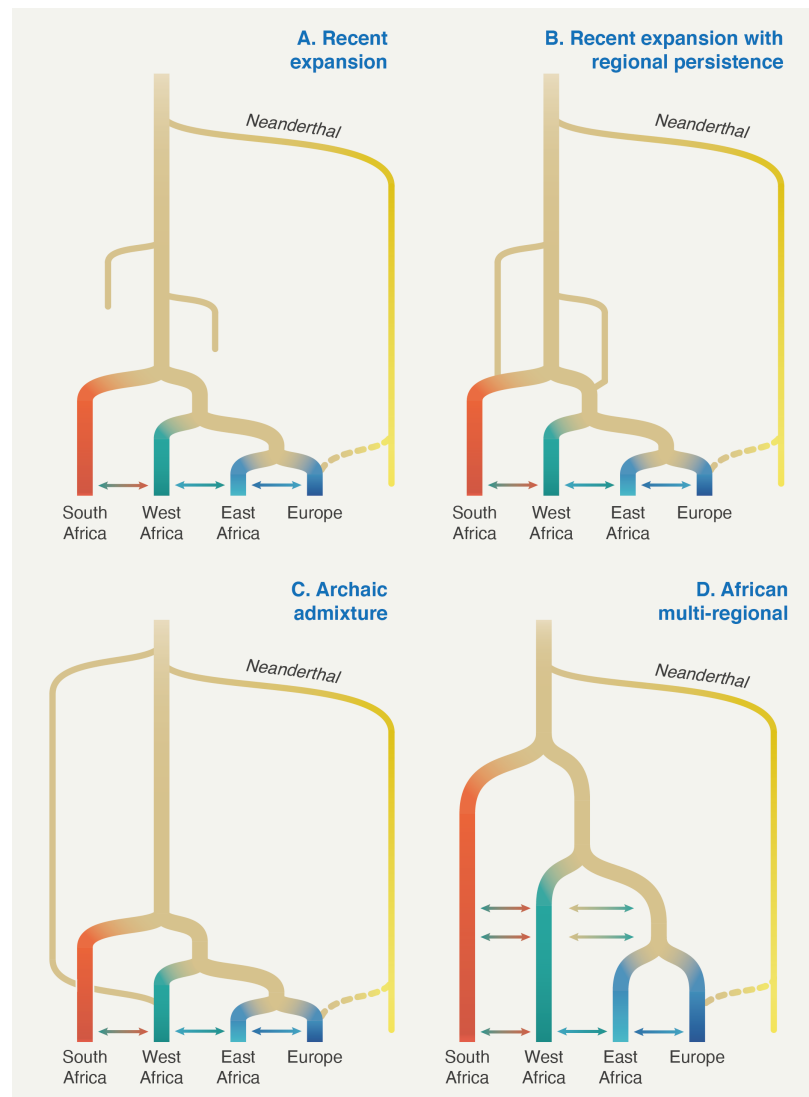


Figure S1: **supp.**